# Land water contribution to sea level from GRACE and Jason measurements

L. Jensen,[1] R. Rietbroek,[1] J. Kusche[1]

L. Jensen, Institute of Geodesy and Geoinformation, Bonn University, Nussallee 17, 53115 Bonn, Germany (jensen@geod.uni-bonn.de)

[1]Institute of Geodesy and Geoinformation, Bonn University, Germany.

**Abstract.** We investigate the effect of water storage changes in the world's major hydrological catchment basins on global and regional sea level change at seasonal and long-term time scales. In a joint inversion using GRACE and Jason-1 data we estimate the time-dependent sea level contributions of 124 spatial patterns ('fingerprints') including glacier and ice-sheet melting, thermal expansion, changes in the terrestrial hydrological cycle and glacial isostatic adjustment. Particularly, for hydrological storage changes we derive fingerprints of the 33 world's largest catchment basins, assuming mass distributions derived from the leading EOFs of total water storage in the WaterGap Global Hydrological Model (WGHM). From our inversion, we estimate a contribution of terrestrial hydrological cycle changes to global mean sea level of $-0.20 \pm 0.04$ mm/yr with an annual amplitude of $6.6 \pm 0.5$ mm for 08/2002 to 07/2009. Using only GRACE data in the inversion and comparing to hydrological changes derived from GRACE data directly using a basin averaging method shows a good agreement on a global scale, but considerable differences are found for individual catchment basins (up to 180%). Hydrological storage change estimates in 33 basins from the GRACE/Jason fingerprint inversion indicate a trend 46% smaller and an annual amplitude 43% bigger compared to WGHM-derived storage changes. Mapping the hydrological trends to regional sea level reveals the strongest sea level rise along the coastlines of South America (max. 0.9 mm/yr) and West Africa (max. 0.4 mm/yr), whereas around Alaska and Australia we find the hydrological component of sea level falling (min. -2.0 mm/yr and -0.9 mm/yr).

## 1. Introduction

The IPCC 4th assessment report (IPCC-AR4, *Bindoff et al.* [2007]) identified sea level change as one of the most important environmental problems for the coming century. Global mean sea level has been observed to rise by $3.4 \pm 0.4$ mm/yr over the last two decades [*Cazenave and Llovel*, 2010], while regional sea level increases by up to three times this number and even falls in some places [*Slangen et al.*, 2012]. Though predictions for regional sea level exhibit considerable variance, it is expected that many low-lying countries will face ecological and economical difficulties associated with sea level rise in the future. Many coastal regions will be affected by for example submergence of land, frequent flooding, saltwater intrusion of surface waters, and increased erosion [*Nicholls and Cazenave*, 2010].

Understanding and quantifying the individual sources that contribute to global mean sea level and regional sea level change is therefore crucial. Ocean warming, an observed melting of (parts of) the large ice sheets and glaciers, and land subsidence due to glacial isostatic adjustment (GIA) all contribute to absolute sea level changes as observed by satellite altimetry. In addition, variability in the terrestrial hydrological cycle affects sea level through net run-off and surface flux changes.

Understanding hydrological variability is particularly important since a large share of it is believed to be caused by anthropogenic activity, i.e. groundwater pumping, irrigation, and reservoir construction. In the IPCC-AR4 the hydrological changes are not included in the estimate of the various contributions to the budget of global mean sea level change. As the discrepancy between the sum of estimated contributions and the observed sea level change is according to this report $0.3 \pm 1.0$ mm/yr for 1993-2003, land water storage changes are assumed to be small ($< 0.5$ mm/yr) or compensated for by unaccounted or underestimated contributions. However, the contribution from terrestrial hydrological changes is likely one of the least well-known contributions in the sea level budget and reducing its uncertainty is an important task in order to find an explanation for the discrepancy between observed and estimated sea level change.

Estimates of changes in terrestrial hydrology can be derived from hydrological models by solving the water balance equation. For example, *Milly et al.* [2003] use the Land Dynamics (LaD, *Milly and Shmakin* [2002]) model to calculate a small positive sea level trend of about 0.12 mm/yr corresponding to land water storage over 1981 - 1998 and 0.25 mm/yr for 1993-1998. By running the ORCHIDEE model over five decades (1948 - 2000) *Ngo-Duc et al.* [2005] find no significant trend but a strong decadal variability of about 2 mm in amplitude. For other time periods, they derive trends of 0.08 mm/yr (1981-1998) and 0.32 mm/yr (1972-1993). Anthropogenic effects are difficult to model due to data scarcity, but studies indicate that these may play an important role [*Fiedler and Conrad*, 2010]. For example, *Chao et al.* [2008] estimate that from dam impoundment alone the sea level could have decreased by 0.55 mm/yr in the last half of the past century. On the other hand, *Konikow* [2011] finds a positive sea level trend of 0.4 mm/yr due to groundwater depletion for 2000 - 2008. A somewhat stronger trend of $0.57 \pm 0.09$ mm/yr due to groundwater depletion is diagnosed for the year 2000 by *Wada et al.* [2012]. In this study it is suggested that groundwater depletion may dominate the terrestrial hydrological contribution to sea level change in future, leading to a net land water contribution of $0.87 \pm 0.14$ mm/yr by 2050. Sea level changes due to anthropogenic impacts on terrestrial water storage are also estimated by *Pokhrel et al.* [2012] for 1961 - 2003 to be 0.77 mm/yr (1.05 mm/yr from groundwater depletion, $-0.39$ mm/yr from dam impoundment, 0.08 mm/yr from climate-driven changes in terrestrial water storage and 0.03 mm/yr from the Aral Sea).

Since the launch of the GRACE (Gravity Recovery And Climate Experiment) satellites in March 2002, land mass changes can be directly observed. By reducing superimposed mass signals (melting of glaciers, glacial isostatic adjustment GIA, atmospheric and oceanic variations), terrestrial hydrological cycle changes can be assessed with GRACE. For example, *Ramillien et al.* [2008] applied a basin averaging method to filtered GRACE Release 3 monthly solutions from the GeoForschungsZentrum Potsdam (GFZ). By considering 27 of the world's largest river basins, they rate the terrestrial hydrological contributions to global mean sea level to $0.19 \pm 0.06$ mm/yr. Using the same method but with GRACE Release 4 data provided by three processing groups (GFZ, Jet Propulsion Laboratory JPL, and Center for Space Research at the Texas University CSR), an extended time period (2002 - 2009), and considering 33 river basins, *Llovel et al.* [2010] estimated the terrestrial hydrological contribution to sea level change to be slightly negative ($-0.22 \pm 0.05$ mm/yr, i.e. more water is deposited on land). Finally *Riva et al.* [2010] assess the total ice and water mass loss from land (including Greenland, Antarctica and glaciers) contributing to $1.0 \pm 0.4$ mm/yr over the years 2003-2009. Of this, they conclude that the net impact of terrestrial hydrology adds (or rather subtracts) a small rate of $-0.1 \pm 0.3$ mm/yr to global mean sea level, but that it dominates regional sea level change in coastal regions.

There are several reasons for the observed differences in the estimated land water storage changes. Whereas in the hydrological models the water storage changes for the entire land area (with Greenland and Antarctica excluded) are considered, *Ramillien et al.* [2008] and *Llovel et al.* [2010] only estimate the contribution of the 27 and 33, respectively, largest river basins. In doing so, areas with strong non-hydrological signals (e.g. glacier melting) which cannot be easily separated from the hydrological signals can be excluded from the estimate. However, since only 43% of the continental surface is covered by those basins, part of the hydrological signal may be neglected. On the other hand, when GRACE-derived mass changes of the entire land surface are compared to hydrological model results, the contribution of glacier melting (usually not part of the model) has to be taken into account. In addition, differences between the estimates derived from GRACE observations may be due to different data releases, different background models (e.g. GIA) and different filtering procedures. Furthermore, due to the strong interannual and decadal variability of water storage, computed trends are strongly dependent on the time period considered and cannot be directly compared. On the other hand, hydrological models are sensitive to errors in forcing fields and water use data. As in particular trends are often not well captured in these data [*Fiedler and Döll*, 2007; *Vörösmarty and Sahagian*, 2000], modelled terrestrial hydrological cycle trends may be quite uncertain.

In theory, one could try to remove all other modelled or observed contributions to global mean sea level or regional sea level from the sea level change as observed by radar-altimetric satellite missions, in order to solve for the contribution of the terrestrial hydrological cycle. This residual approach, however, proves difficult as considerable uncertainties are associated with all other contributions as well [*Milne et al.*, 2009; *Chambers and Schröter*, 2011]. The same holds for conventional basin averaging approaches performed on GRACE data, in which all superimposed mass signals have to be removed prior to analysis. In the present contribution, we provide a new estimate for land water contributions to global and regional sea level rise based upon data from the GRACE mission and the Jason-1 altimeter satellite. Like *Llovel et al.* [2010], we consider the 33 world's largest hydrological catchment basins. We use a fingerprint method first suggested by *Plag and Jüttner* [2001] in the context of tide gauge data analysis which is based on the assumption that the large-scale sea level patterns of the major sources of sea level change can be well-modelled using physical relations except for a time-variable magnitude, that determines the actual sea level contribution of the source. To assess these magnitudes we combine temporal gravity and altimetry data in a joint least squares inversion. Whereas the fingerprints are pre-defined and assumed to be time-invariant, the gravity and altimetry data is (solely) used to estimate the time-series of scaling factors for the fingerprints, and not for determining the spatial pattern. In contrast to other observation-based estimates, we jointly assess all contributions (including the steric effect) to sea level change and therefore do not rely on models of superimposed signals to be removed. Another advantage of our method is that filtering and rescaling of the GRACE data, a major source of uncertainty in GRACE-derived mass changes, can be avoided. We demonstrate this by applying our method to GRACE data only (without considering altimetry data) and comparing to results obtained with a conventional GRACE basin averaging approach. We also compare our results to water storage changes from the WaterGAP Global Hydrological Model (WGHM, *Döll et al.* [2003]) both on basin and continental scale. Furthermore, we use the fingerprint inversion to map the regional sea level change caused by water storage changes in the 33 largest basins and estimate the impact on the three largest ocean basins.

This paper is organized as follows: In section 2 we describe the three methods - hydrological modelling, GRACE basin averaging and the fingerprint inversion - which we use to derive the terrestrial hydrological cycle change estimates. The used data and preprocessing steps are specified in section 3. In section 4 we discuss our results with emphasis on the contribution of the 33 largest catchment basins to global mean sea level change obtained with different methods and the regional sea level change. In section 5 we draw the conclusions from our results and address future work.

## 2. Methods

### 2.1. Hydrological modelling

Sea level contributions caused by terrestrial hydrological changes can be evaluated using land surface models or global hydrological models. In-situ measurements of groundwater levels and other hydrological storage systems are temporally and spatially sparse, and may be biased when collected in areas where the water table is locally lowered due to irrigation. Models are forced by meteorological data and aim at realistic physical or conceptual process representation, transfer of energy, lateral and vertical flux of water, and anthropogenic water use. They may be calibrated against gauged runoff. When aggregated over vertical compartments and grid cells or catchments, mass conservation states that the change of mass over land, $\frac{dM}{dt}$, originates from the net effect of precipitation, $P$, evaporation, $E$ and runoff, $R$:

$$\frac{dM}{dt} = P - E - R. \tag{1}$$

However, biases in observed forcing fields, deficiencies in model realism and physical parametrization, and missing information on water consumption, irrigation, reservoir building and other factors may render long-term storage change and aggregated runoff unrealistic. In this work, we assume that the right-hand side of Eq. (1) reaches the ocean immediately [*Peixoto and Oort*, 1992], and that it adapts itself to an equipotential surface. With other words, on the spatial and temporal scales considered here, changes of the amount of water stored in the atmosphere will be neglected as well as dynamic effects of ocean circulation.

### 2.2. GRACE basin averaging

GFZ Potsdam, JPL, CSR, and a number of other groups provide time-dependent Stokes' coefficients $c_{nm}(t)$, $s_{nm}(t)$ derived from GRACE observations. From these, one can derive surface mass variations $\frac{dM}{dt}$ using methods described for example in *Wahr et al.* [1998] and thus compute the left-hand side of Eq. (1). Usually, the temporal resolution is one month. Since GRACE cannot separate between different sources of mass variability, all non-hydrological signals (atmosphere, ocean, glaciers, GIA) have to be reduced from the data in order to isolate the hydrological mass variations. Moreover, the spatial resolution of the GRACE-derived mass variations is limited to about 300 km due to the altitude of the satellites and the accuracy of the microwave ranging instrument. Therefore realistic terrestrial hydrological mass variations can only be estimated as an average for basins larger than about 90000 km$^2$.

For higher spherical harmonic degrees, the GRACE coefficients are strongly affected by correlated errors, which cause characteristic north-south directed artifacts in the spatial domain. Hence, to derive realistic mass variations, filtering of the monthly solutions is necessary. Usually a spectral decorrelation followed by a spatial smoothing is applied [*Swenson and Wahr*, 2006; *Kusche*, 2007]. Filtering the GRACE data reduces noise but it also leads to an amplitude attenuation of the signal and external mass signals leaking into the averaging area (leakage-in). The amplitude attenuation is often compensated for by rescaling the mass variations with a constant factor (e.g., *Velicogna and Wahr* [2006]). However, as the true mass distribution and thus the true attenuation is unknown, the determination of the rescaling factor always involves assumptions [*Kusche*, 2007; *Klees et al.*, 2008; *Fenoglio-Marc et al.*, 2012]. There exist several methods for reducing the leakage-in caused by external mass variations, which also involve their own assumptions [*Baur et al.*, 2009; *Longuevergne et al.*, 2010]. Handling these two effects is one of the major source of uncertainties in GRACE-derived basin averages.

To obtain regional sea level changes, the computation of sea level fingerprints is required. Assuming a normalized load distribution in the basin and applying the sea level equation (e.g. appendix A1) to it leads to a spatial sea level pattern, which is - scaled with the GRACE basin average - an estimate for regional sea level changes. A similar approach, pursued by *Riva et al.* [2010], is to derive global maps of mass trends from GRACE data and use these as the input load for the sea level equation.

### 2.3. Fingerprint inversion from GRACE

The idea of our fingerprint inversion is that the total (observed) sea level change pattern consists largely of a sum of characteristic spatial patterns of sea level change caused by individual mass sources $M_{(i)}(\lambda, \theta)$. It is assumed that these fingerprints can be calculated a priori up to an unknown time-dependent magnitude for each fingerprint. By combining gravity and altimetry data the magnitudes can be estimated. In contrast to mascon approaches [*Rowlands et al.*, 2010], where patterns are defined on a (regular) grid, our fingerprints result from the physical delineation of a limited number of independent regions and their individual mass distribution. In our current approach, the fingerprints are assumed to remain constant over time, merely the scaling factor (magnitude) is time-variable. Ocean model simulations may be used in future to constrain the time scales where this working hypothesis is valid [*Brunnabend et al.*, 2011].

The fingerprints can be calculated in terms of sea level but also in terms of the associated gravitational potential. Thus we assume that the total gravitational potential observed by GRACE consists of a sum of characteristic spatial patterns of gravitational potential scaled with the same (to be solved for) magnitudes as the corresponding sea level fingerprints. Whereas the fingerprints for different mass sources have to be calculated by using the full sea level equation, involving gravitational-elastic response and rotational feedback [*Rietbroek et al.*, 2011], their magnitudes (i.e. the scaling factors), are solved-for parameters of the inversion. They can be estimated by fitting the Stokes' coefficients $c_{nm}^{(i)}$, $s_{nm}^{(i)}$ that we derive from the pre-computed fingerprints to the GRACE-derived Stokes' coefficients by means of a least squares inversion. In order to consider only signals of global mean sea level contributors, atmospheric signals have been removed from the GRACE data in advance.

When fitting the relatively large-scale fingerprints to the GRACE level-2 data in terms of potential no further smoothing or destriping of the GRACE coefficients is required. Using GRACE level-2 data, we estimate magnitudes $x(t)$ of the fingerprints for ice sheet (Greenland, Antarctica) basins, a set of clusters of glaciers, hydrological catchments (including lakes and groundwater contributions) and an a priori chosen global GIA pattern by solving

$$\delta\Phi(t) = A \begin{pmatrix} x_{ice} \\ x_{glac} \\ x_{hydro} \\ x_{gia} \end{pmatrix} (t) + e(t), \tag{2}$$

where $\delta\Phi(t)$ are the (stacked) Stokes' coefficients measured by GRACE. Columns of the design matrix $A$ contain the Stokes' coefficients $c_{nm}^{(i)}$, $s_{nm}^{(i)}$ of the fingerprints and the vector $e(t)$ represents the GRACE errors and the 'ommission' error of variability not explained by our set of source patterns. We then set up normal equations with normal matrix, $N_G$ and right hand side, $n_G$:

$$N_G(t) = A^T C_G^{-1}(t) A \qquad n_G(t) = A^T C_G^{-1}(t)\delta\Phi(t) \tag{3}$$

where $C_G^{-1}(t)$ is the inverse error covariance matrix of the GRACE Stokes' coefficients $\delta\Phi(t)$. As the GRACE Stokes' coefficients $\delta\Phi(t)$ already represent the solution of the original GRACE normal equations

$$\delta\Phi(t) = (N^*)^{-1}(t) n^*(t) \tag{4}$$

(to which we have access), the inverse error covariance matrix in (3) is given by $C_G^{-1}(t) = N^*(t)$. With other words, our normal equations follow from a re-parametrization of the GRACE normal equations,

$$N_G(t) = A^T N^*(t) A \qquad n_G(t) = A^T n^*(t). \tag{5}$$

Before solving for $x(t)$ the normal equations can be modified. The temporal resolution of the resulting time series can be stabilized by accumulating several normal equations. As in this study we are mainly interested in trend and seasonal variations of mass changes, we modified the normal equations by inserting parameters for trend and annual sine and cosine wave amplitudes for each fingerprint and accumulating all normal equations in the time period August 2002 until July 2009.

Within the fingerprint method small neighboring basins cannot be separated, because they exhibit very similar fingerprints. However, in contrast to the GRACE basin averaging method, here we obtain correlations for the mass variations between the different basins and thus get information about dependencies of basin mass estimates. Due to the coarse GRACE spatial resolution, one has to limit the set of patterns or base functions to those of larger spatial extent and avoid near rank defects in an inverse scheme as suggested here. On the other hand, patterns of mass flux or sea level change that we disregard in the inversion, such as ocean circulation changes, water storage changes outside of the 33 basins or individual glaciers, may bias our results depending on their degree of spatial non-orthogonality with respect to the patterns that are modelled. This 'representation error' effect has a similar nature as the leakage-in problem in a basin averaging approach.

### 2.4. Fingerprint inversion from GRACE and Jason-1

Several years ago, *Plag and Jüttner* [2001] suggested to use tide gauge observations of sea level in a fingerprint inversion approach. Similarly, radar altimetric missions allow measuring global sea level directly. However, altimetric sea level also contains steric height changes and a component due to the dynamic ocean circulation. The consistent separation of sources of sea level change therefore calls for combining the two observation techniques GRACE and altimetry [*Rietbroek et al.*, 2011].

We may relate the fingerprint magnitudes $x(t)$ to the Jason-1 along-track sea level anomalies $\delta h(t)$ by

$$\delta h(t) = B \begin{pmatrix} x_{ice} \\ x_{glac} \\ x_{hydro} \\ x_{gia} \\ x_{ster} \end{pmatrix} (t) + e(t) \tag{6}$$

similar to Eq. (2). Matrix $B$ contains in its columns the normalized fingerprints evaluated at the measurement locations. The vector $e(t)$ accounts for altimeter noise (range and correction errors) and ocean variability beyond a 'passive' ocean response [*Blewitt and Clarke*, 2003]. From the Jason-1 data, we set up a second system of normal equations

$$N_J(t) = B^T C_J^{-1}(t) B \qquad n_J(t) = B^T C_J^{-1}(t) \delta h(t) \tag{7}$$

weighted by the matrix $C_J(t)$ containing the Jason-1 errors. Equations (7) are then combined with the normal equations obtained from GRACE observations (Eq.(5)) and subsequent inversion provides the fingerprint magnitudes for all contributors to sea level change. Combining GRACE and Jason is useful, since the nullspace of the combination is smaller than the nullspace of each technique. E.g., *Rietbroek et al.* [2011] determined secular geocenter motion from this combination (see also *Wu et al.* [2012]).

At present $C_G(t)$ in equation (3) and $C_J(t)$ in equation (7) are modelled to represent instrumental errors only and are considered thus both too optimistic. In future research we will try to assess more realistic weighting which will include assessing unmodelled variability and omission errors. Whereas $C_G(t)$ is derived from the full GRACE covariance matrix and therefore takes into account spatial correlations, the errors in $C_J(t)$ are calculated from the standard deviations of the 20 Hz satellite observations and no correlations are considered.

## 3. Data

### 3.1. WGHM data

In this study, we use global, monthly variations of total water storage (TWS) derived from the WaterGAP Global Hydrological Model (WGHM, *Döll et al.* [2003]). WGHM simulates the terrestrial water cycle by implementing conceptual formulations of the most important hydrological processes and includes all storage compartments relevant for describing vertical and lateral mass redistribution. The model is forced by ECMWF climate data (temperature, cloudiness, number of rain days) and GPCC monthly precipitation data [*Rudolf and Schneider*, 2005], and calibrated against gauged runoff. It has been used in many GRACE-related studies and has been calibrated against GRACE by *Werth and Güntner* [2010]. Furthermore, specific model versions exist that consider updated anthropogenic water use [*Döll et al.*, 2011], improved floodplane dynamics [*Adam et al.*, 2010], or higher spatial resolution ($5' \times 5'$, *aus der Beek et al.* [2011]). Here, we use $0.5° \times 0.5°$ output fields of WGHM provided by *Döll et al.* [2011], with the long-term average TWS removed to obtain anomalies comparable to GRACE results. Unrealistic values and trends have been observed in some regions (for example in Greenland), but these are not included in our inventory of the largest 33 basins.

### 3.2. GRACE data

For the basin averaging method, we use GRACE Release 4 Level 2 monthly solutions provided by GFZ Potsdam for the time period July 2002 to August 2009, given in form of Stokes' coefficients up to degree and order 120 [*Flechtner*, 2007]. The monthly solutions are reduced for atmospheric and oceanic signals using standard Atmosphere and Ocean De-aliasing Level-1B (AOD1B) products. As is well-known, degree 1 coefficients related to geocenter motion cannot be observed from GRACE range rates. However, as the individual precomputed fingerprints contain contributions from the degree 1 coefficients, the fingerprint inversion from GRACE provides a time-series of degree 1 coefficients by which we augment the GRACE monthly solutions before using them in the basin averaging approach. Moreover, in the GRACE Release 4 monthly solutions the $c_{20}$ coefficient is affected by ocean tidal aliasing and exhibits large non-geophysical variations. Therefore we replace $c_{20}$ with an external time-series derived from SLR measurements [*Cheng and Tapley*, 2004]. Then, we remove the average of the monthly solutions over the whole time-period to obtain anomalies. Before averaging over the basins we destripe the monthly solutions by applying the anisotropic DDK3 filter [*Kusche*, 2007]. We account for the effect of GIA by subtracting a model by *Klemann and Martinec* [2009] which uses the ICE-5G ice history and VM2 rheology [*Peltier*, 2004], and which is given in spherical harmonic coefficients up to degree and order 64.

For the fingerprint inversion method, we use weekly GRACE Release 4 normal equations from GFZ Potsdam complete up to degree and order 150 [*Dahle et al.*, 2008], processed with the same standards as the monthly solutions. In order to be consistent with altimetry data, the weekly AOD1B products as well as rates in the $c_{20}$ and $c_{40}$ coefficients are restored. However, to be consistent with the IB-correction from altimetry, we do not restore the ocean average of the atmospheric pressure over the ocean [*Leuliette and Miller*, 2009]. The weekly GRACE normal equations do not contain degree 1 coefficients. In contrast to the basin averaging method, we do not use external time-series for degree 1 coefficients within the fingerprint inversion method, as these can be estimated [*Rietbroek et al.*, 2011]. Furthermore, there appears no need for filtering or smoothing the weekly GRACE normal equations in the fingerprint inversion method because the GRACE data do not provide the spatial patterns of mass variations but are rather projected onto the 'fingerprint space'.

### 3.3. Jason-1 data

The Jason-1 [*Chambers et al.*, 2003] data is obtained from the Open Altimeter Database (OpenADB, *Schwatke et al.* [2010]). The altimeter ranges in this database were interpolated to predefined bins which are located alongtrack and are fixed in time and space. The size of the bins corresponds to the length of the path that the satellite ground track covers in one second, i.e. about 5.8 km. OpenADB data is corrected for several geophysical and atmospheric effects: the EOT11a model is used for ocean and loading tides, and a dynamic atmospheric correction based on AVISO products using the Mog2D model for high frequencies and an inverse barometer correction for the lower frequencies is applied. Dry troposphere effects are corrected using reanalysis data from the European Centre for Medium-range Weather Forecast (ECMWF), whereas the wet troposphere effect is derived from the radiometer data of the satellite. Jason-1 orbits refer to the EIGEN-GL04c gravity field model and are expressed in the ITRF2005 reference frame. Radial orbit errors are derived from comparing multi-mission altimetry (MMXO12 cross calibration).

We did not apply a GIA correction to the altimeter data, since we include it within the fingerprint inversion where the GIA contribution is estimated together with other sea level contributions.

### 3.4. Steric data

In this study, the steric sea level contribution is estimated indirectly in the fingerprint inversion by combining Jason-1 and GRACE data. To separate steric from mass induced sea level changes we calculate fingerprints not only for the mass contributions but also for the steric contributions. The steric fingerprints are derived from gridded in-situ data from Argo floats, bouys and CTD casts: we use a dataset from *Hosoda et al.* [2008] who provide monthly global 1° grids of steric sea level height. Since the Argo data (temperature and salinity) are collected up to a maximum depth of 2000 m, the contribution of possible deep ocean warming is not contained in the datasets. We perform a Principle Component Analysis (PCA) on the monthly grids for the time period 01/2001 to 10/2010, and the first 30 Empirical Orthogonal Functions (EOFs) are then used as steric fingerprints in the inversion. These 30 EOFs contain about 87% of the total signal. To summarize, we would like to emphasize that in this study we do not use the Argo data directly to quantify the steric sea level contribution but only derive the spatial patterns from these data, while the magnitudes of the patterns are indirectly estimated by combining altimetry and GRACE in the fingerprint inversion.

## 4. Results

### 4.1. Global sea level change from 33 basins

For this study, we consider the 33 largest river basins of the world (Fig. 1). Their outlines are based on masks with 0.5° resolution from *Oki and Sud* [1998]. Analysis of the WGHM water storage shows that these basins nevertheless capture only 48% of the annual amplitude and 74% of the trend of the total hydrological signal represented by the model. However, the regions not covered by these 33 largest basins are mainly regions which are either known to exhibit small storage changes (North Africa, Arabian Peninsula, Western Australia), contain glaciers (e.g. Patagonia, Himalaya), or are highly affected by GIA uplift (Fennoscandia, Canada). Since models of glacier mass loss and GIA are subject to large uncertainties [*Cogley*, 2009; *Guo et al.*, 2012], basin averages of hydrological changes obtained from GRACE in those regions will be highly uncertain. Although in principle the fingerprint inversion method should allow to better distinguish superimposed signals as long as they are related to different spatial patterns, here we use only the 33 basins in order to be comparable with the GRACE basin averaging results.

#### 4.1.1. Results from the GRACE basin averaging

The GRACE basin averages for the time period August 2002 to July 2009 are computed in the spectral domain by converting the basin masks into spherical harmonic coefficients and accumulating the product of these coefficients with the filtered GRACE coefficients, converted to equivalent water height (EWH) following *Wahr et al.* [1998]. To account for an amplitude attenuation [*Klees et al.*, 2008] due to filtering, we rescaled the monthly averages with a factor, which we compute separately for each basin: We convert a uniform basin mass distribution into spherical harmonic coefficients and filter them with the same filter as applied to the GRACE coefficients. The scaling factors - the ratio of the average basin mass before and after filtering - range between 1.08 and 1.75. The trends, phases and annual amplitudes obtained for the terrestrial hydrological mass change with the GRACE basin averaging (in the following abbreviated as *BasAv*) after rescaling are shown in column 3 (*BasAv*) of table 1 and 2. For the phase we indicate the month in the year when the maximum of the annual variation is reached.

Three main error sources add to the uncertainty of these values: the choice of the filter, the choice of the GIA model (only influencing the trend) and the GRACE measurement errors. To account for the error introduced by filtering and rescaling, we compute the total terrestrial hydrological trend, annual amplitude and phase from GRACE monthly solutions with five different filters (DDK1, DDK2, DDK3, Gaussian 300km, Gaussian 500km). Each time series is rescaled corresponding to the filter that was used. By comparing, we obtain RMS values of 9.9 Gt/yr for the trend, of 212.2 Gt for the annual amplitude, and of 0.03 months for the phase. We compare the contribution of four different GIA models [*Klemann and Martinec*, 2009; *Spada and Stocchi*, 2007; *Wang et al.*, 2008; *Wu et al.*, 2010] to mass change in the region covered by all 33 basins and find a RMS of 12.7 Gt/yr adding to the uncertainty of the trend. The uncertainty due to GRACE errors propagated from the calibrated errors of the GRACE monthly solutions is found to be 3.3 Gt/yr, 28.3 Gt and 0.02 months for trend, amplitude and phase, respectively. Thus, these three error levels yield the error bars finally given in tables 1 and 2 for the total values.

### 4.1.2. Results from the GRACE-only fingerprint inversion

Within the fingerprint inversion method, we precompute 124 fingerprints: 16 fingerprints for Greenland drainage basins, 31 fingerprints for Antarctica drainage basins, 13 fingerprints for clusters of major glacier systems (from the World Glacier Inventory WGI, *NSIDC* [1999]), 33 river basin fingerprints for the terrestrial hydrological cycle, 1 fingerprint for the GIA contribution, and 30 fingerprints for the steric contribution. The fingerprints are calculated as follows: For the mass contributions, we use the sea level equation [*Farrell and Clark*, 1976] to derive mass consistent fingerprints in terms of sea level and in terms of gravitational potential, see also appendix A1. We normalize the mass load used in the sea level equation for each source to 1 Gt. In particular, the 33 terrestrial hydrological fingerprints are derived by applying the sea level equation assuming a uniform mass change in each of the largest river basins. For the GIA pattern we use the same model by *Klemann and Martinec* [2009] as considered in the GRACE basin averaging. As described in section 3.4 for the steric sea level patterns, we perform a Principal Component Analysis (PCA) of gridded products derived from Argo and other in-situ data [*Hosoda et al.*, 2008] and use the first 30 EOFs as steric 'fingerprints' [*Rietbroek et al.*, 2011].

As mentioned above, to separate the effect of methodology (fingerprint inversion vs. basin averaging) from the sensitivity with respect to the added altimetry data, we first performed a fingerprint inversion with only GRACE data (below referred to as $InvGR$). In this case, we did not incorporate the steric fingerprints. Although it is theoretically possible in the fingerprint inversion from GRACE to estimate a scaling factor for the GIA model, here we fixed this factor to 1.0 in order to be consistent with the basin averaging method. By augmenting the weekly normal equations of the fingerprint inversion by trend and sine/cosine wave parameters for each fingerprint, and adding up all normal equations for the considered time period, we estimate the values for the terrestrial hydrological cycle changes listed in column 4 ($InvGR$) of table 1 and 2. Uncertainties for these values are obtained from the formal inversion errors scaled with the a posteriori variance; however they appear to be underestimated by about a factor of 10 compared to the errors of the GRACE basin averaging.

The total terrestrial hydrological cycle trends and annual amplitudes obtained with the two methods (basin averaging and fingerprint inversion from GRACE data only) differ by 14.4% and 4.1%, respectively and agree within their standard deviations. The absolute phase difference is found to be 0.05 months. However, the relative difference of the trends for individual basins can be quite large (maximum 171.1% for Danube, minimum 0.2% for St. Lawrence). The mean relative difference is 62.5% for the trend and 33.9% for the amplitude. The RMS of the phase differences is rather small, only 0.29 months. Analysis of the relative differences for individual basins showed that the magnitude of the differences depends neither on the basin size nor on the geographical latitude of the basin. Comparing the trends accumulated to the continental scale (table 3) shows that big differences mainly occur in the North American and Eurasian basins, where large glaciers and GIA signals are superimposed to hydrological signals. Whereas in the inversion method the mass variations of glaciers are simultaneously estimated and correlations can be evaluated, they are not considered in the basin averaging method. Another difference in the methods is the filtering of the GRACE data, which is omitted in the inversion method. On the other hand in the basin averaging method, no predefined information about the spatial pattern of the mass variations is used, whereas in the inversion we assume the mass variations to be uniform in each hydrological basin, which is likely not the case for large basins.

#### 4.1.3. Results from the combined GRACE/Jason-1 fingerprint inversion

Column 5 ($Inv$) of table 1 and 2 shows the results of the combined GRACE and Jason-1 fingerprint inversion, i.e. with using GRACE and Jason-1 normal equations and co-estimating the magnitudes for the steric fingerprints. For better comparison with the GRACE-only fingerprint inversion, we still set the GIA factor to 1.0 and use uniform mass distribution for the calculation of the basin fingerprints. Somewhat surprisingly, introducing Jason-1 data causes a sizeable effect on the estimated total trend of the hydrological basins (difference 71.9% between $InvGR$ and $Inv$), whereas amplitude and phase do not change much (difference 3.1% and 0.10 months). Interestingly, the other mass-related contributors to global mean sea level change (Greenland, Antarctica, Glaciers) are much less affected by adding the altimetry data. Whereas the terrestrial hydrological cycle trends obtained with different inversion schemes exhibit a global mean sea level standard deviation of 0.066 mm/yr, trends for Greenland, Antarctica and the Glaciers result with standard deviations of only 0.003, 0.010 and 0.038 mm/yr, respectively. This phenomenon is currently being investigated. Relative differences of individual basin trends, amplitudes and phases with respect to the basin averaging method are similar to those from the GRACE-only inversion (69.2% and 32.5% in average for trend and amplitude, respectively; 0.05 months for the phase).

As mentioned above, the mass change in the hydrological basins is not uniform as assumed in the results discussed so far. Using a more realistic mass distribution might thus reduce the trend differences of the basins between the two methods. To study this effect, we calculated fingerprints from the leading EOFs (Empirical Orthogonal Functions) of each basin's WGHM output maps. Using these fingerprints in the combined inversion instead of those produced from uniform mass distributions we estimate a total trend of

54.1 Gt/yr for the terrestrial hydrological cycle (not shown in table 1 and 2) which is closer to the *BasAv* and the *InvGR* solutions than the terrestrial hydrological trend of the *Inv* solution. However, the mean relative difference of the basins (70.6%) did not improve. The reason might be that the leading EOFs, pointing in the direction of maximum variability of the data, may not be well suited to represent trends. Strikingly, the trend of the Amazon basin is found much smaller (only 39.8 Gt/yr) than estimated from the other solutions (101.9, 82.7 and 67.2 Gt/yr, respectively). The annual amplitude of the Amazon basin is also smaller for the solution using hydrology EOFs than for the others (1086.8 Gt vs. 1171.0, 1312.5, and 1306.1 Gt respectively). The Amazon basin might be too big to be well described in its spatial mass change variability by only one EOF. In fact, the Amazon basin is nearly twice as big ($6.23 \times 10^6$ km$^2$) as the largest of the other basins (Congo, $3.76 \times 10^6$ km$^2$) we considered. Using two hydrological EOF-fingerprints for the Amazon basin in the inversion (and one EOF for the other basins) leads to a trend and amplitude of the Amazon basin (66.7 Gt/yr and 1207.0 Gt) that are closer to those of the other solutions while the other basins are nearly unaffected. The results of this inversion are shown in column 6 (*InvEOF*) of table 1 and 2. In this solution, we also co-estimated a scaling factor of 0.97 for the GIA pattern instead of fixing it to 1.0 which is well within the spread of current GIA models. The total terrestrial hydrological cycle trend is now similar to the GRACE-only trend (*InvGR*) and it is 16.1% smaller than the hydrological trend of the *BasAv* solution, while the amplitudes of the two solutions differ by only 1.4% with an absolute phase difference of 0.06 months.

As mentioned above, error estimates obtained with the inversion method are probably too optimistic. As an upper boundary for the errors of trend, amplitude and phase, we calculate the standard deviations of the results from the different inversion setups in table 1 and 2 to 31.3 Gt/yr, 48.0 Gt and 0.06 months, respectively. Whereas for amplitude and phase this seems to be realistic, for the trend it appears too pessimistic in comparison to the *BasAv* errors. Being conservative, we scale the errors from the inversion by a factor of 10 in order to match the magnitude of the *BasAv* errors.

#### 4.1.4. Results from the WGHM

For comparison, we also computed the trends, annual amplitudes and phases of the terrestrial hydrological mass change for the time period August 2002 to July 2009 from WGHM alone. The results are shown in column 7 of table 1 and 2, respectively. Whereas the total terrestrial hydrological trend obtained from the WGHM is 45.9% larger than the *BasAv* trend, the seasonal amplitude is 43.2% smaller. We also find a sizeable absolute phase difference of 1.17 months. Differences compared to the trends estimated within the inversion are even bigger, up to 87.0%. The relative differences of individual basin trends between the WGHM and the *BasAv* solution can reach up to 148.6% and the average difference is 79.4%. For the amplitude, the maximal relative difference is 77.6% with an average difference of 44.5%. Absolute phase differences range from 0.1 to 4.2 months for the individual basins with an RMS of 0.27 months. Other authors also found significant discrepancies between mass changes derived from GRACE and from WGHM [*Werth and Güntner*, 2010; *Forootan et al.*, 2012]. Comparing the terrestrial hydrological trends on a continental scale (table 3) shows that the main differences occur in North America and Australia. In North America a strong GIA signal exists, which is present in the GRACE data but not in WGHM. For Australia *Forootan et al.* [2012] found that the correlation between GRACE-derived and WGHM-derived TWS from 2003 to 2010 is significantly lower than for a regional hydrological model. In particular, in the Southeast of Australia (location of Murray and Lake Eyre basin) they found a correlation with the WGHM of mostly below 0.2. This corresponds to part of the differences between WGHM and GRACE-derived terrestrial hydrological cycle trends we find.

#### 4.1.5. Contributions to global mean sea level from the fingerprint inversion

For our reference inversion using GRACE and Jason-1 observations, EOF hydrology fingerprints (two for the Amazon basin) and freely co-estimating a GIA scaling factor, we estimate a total terrestrial hydrological cycle mass trend of $74.7 \pm 13.6$ Gt/yr with an annual amplitude of $2442.6 \pm 204.0$ Gt. We consider this our most realistic estimate. This positive mass trend corresponds to a small negative contribution to global mean sea level change of $-0.20 \pm 0.04$ mm/yr for the period August 2002 to July 2009. The annual amplitude is estimated to be $6.6 \pm 0.5$ mm. However, all terrestrial hydrological cycle trend results are strongly dependent on the time period considered. Taking four different time periods (08/2002 - 07/2009, 01/2003 - 12/2009, 08/2003 - 07/2010, and 01/2004 - 12/2010), using the same inversion setup we found the total terrestrial hydrological cycle trends ranging from $-9.3$ Gt/yr to 92.8 Gt/yr with a standard deviation of 48.2 Gt/yr. The annual amplitude is only marginally affected (2442.6 Gt to 2542.5 Gt, standard deviation of 41.8 Gt). The terrestrial hydrological cycle exhibits strong interannual and decadal variations [*Ngo-Duc et al.*, 2005; *Llovel et al.*, 2010]. The sensitivity of the trend estimates to different time periods is a result of these decadal variations. For Greenland, West Antarctica and glaciated regions the interannual and decadal mass variability is smaller compared to the annual and long-term signal, thus the sensitivity to the time period is less pronounced.

For our reference fingerprint inversion (using one/two EOF WGHM fingerprints and co-estimating the GIA-scale, *InvEOF* in table 1 and 2), using GRACE and Jason-1 data, we calculate the global mean sea level contributions given in column 2 of table 4. To enable a consistent comparison of the total sea level trend from the fingerprint inversion and the total sea level trend obtained from Jason-1 data, we provide in column 3 of table 4 the mean sea level trend for each contributor confined to latitudes between 66° north and 66° south, as the altimeter data also does not cover the high latitudes. The GIA contribution is however kept constant for both columns, since it can be considered as a globally uniform offset of the altimetry data. The altimeter is sensitive to GIA related changes in ocean basin volume, regardless of its data coverage. For 08/2002 to 07/2008 we obtain from the fingerprint inversion a global mean sea level trend of 1.56 mm/yr and from the Jason-1 data a trend of 1.94 mm/yr which leaves 0.38 mm/yr that cannot be explained in the inversion to be due to glacier or ice sheet mass loss, terrestrial hydrological changes, GIA or thermal expansion. The Greenland contribution of $0.63 \pm 0.008$ ($-232.9 \pm 0.3$ Gt/yr) lies within the range of estimates other authors made for similar time periods (*Ewert et al.* [2012], $-191.2 \pm 20.9$ Gt/yr for 08/2002 to 06/2009, *Velicogna* [2009], $-230 \pm 33$ Gt/yr for 04/2002 to 02/2009, *Schrama et al.* [2011] $-201 \pm 19$ Gt/yr for 03/2003 to 02/2010). The contribution of Antarctica $0.26 \pm 0.014$ ($-94.5 \pm 0.5$ Gt/yr) is found to be significantly smaller than the Greenland contribution. This is confirmed in other studies (*Horwath and Dietrich* [2009], $-109 \pm 48$ Gt/yr for 08/2002 to 01/2008, *Velicogna* [2009], $-143 \pm 73$ Gt/yr for 04/2002 to 02/2009). Estimates for the total contribution of glacier ice melting to global mean sea level cover a relatively wide range. In the IPCC-AR4 it is assumed to be $0.77 \pm 0.22$ mm/yr for 1993 to 2003, whereas *Cogley* [2009] find a value nearly twice that big ($1.4 \pm 0.2$ mm/yr) for 2001 to 2005. However, a recent study by *Jacob et al.* [2012] estimated the glacier contribution to global mean sea level to be only $0.41 \pm 0.08$ mm/yr for 2003 to 2010. Thus our estimate of $0.58 \pm 0.027$ mm/yr indeed confirms a rate at the lower end of the published spectrum of estimates. The estimates of the steric and GIA contribution estimate of $0.35 \pm 0.022$ mm/yr and $-0.16 \pm 0.003$ are also consistent with results from other authors [*Cazenave and Llovel*, 2010; *Guo et al.*, 2012]. Our estimate for the contribution of the terrestrial hydrological cycle is discussed in section 5.

### 4.2. Regional sea level change

By converting the basin EOF fingerprints, scaled from the inversion, to the spatial domain we obtain a global map of regional sea level trend and annual amplitude caused by terrestrial hydrological cycle mass changes, which is shown in figure 2. According to our results, mainly the coastal areas of South America as well as the western coast of Africa are affected by a relevant sea level rise due to land water contributions. In the Amazon river delta the trend reaches values up to 0.9 mm/yr, while in the Congo river delta the maximum trend is 0.4 mm/yr. In contrast, the North American coastal area, especially around Alaska, is subject to falling sea level. The minimum of the trend in this area is $-2.0$ mm/yr in the Gulf of Alaska. However, it is unclear to what extent the strong negative regional sea level trend is really caused by hydrological mass changes or by glacier mass loss in the same area. In fact, from the covariance matrix of the inversion a rather strong negative correlation of $-0.55$ between the Yukon basin trend and the Brooks Range glaciers in Northern Alaska is found. The correlation of the Yukon basin with the glaciers at the Gulf of Alaska is $-0.42$. Figure 2 also suggests a sea level fall of minimal $-0.9$ mm/yr around Australia due to mass loss in the Lake Eyre and Murray river basin in the considered time period. Eurasia is only marginally affected by sea level variations due to terrestrial hydrological cycle mass changes.

The annual amplitude shown in figure 2 exhibits for most parts of the northern hemisphere amplitudes below the global mean of 6.6 mm, whereas in the southern hemisphere amplitudes slightly higher than the global mean are predominant. Lower amplitudes in the northern hemisphere are due to the fact that the annual cycle of water mass storage on the northern continents reaches its maximum in mid-March, causing a gravitational attraction of ocean water masses which is nearly 180° out of phase to the globally averaged cycle of ocean water mass (maximum in mid-October). In short, a damping of the amplitude occurs. Analogously, the amplitude increases where the continental mass storage cycle is in phase with the global mean ocean mass cycle. This effect is especially large around South America (with amplitudes down to 1 mm) and Southeast Asia (with amplitudes up to 20 mm) where strong annual mass amplitudes in the Amazon and Mekong basin due to seasonal Monsoon rainfall occur. Depending on the phase of the continental signal, the sea level amplitude is reduced (Amazon) or amplified (Mekong).

Finally, in table 5 we average estimated regional hydrological sea level trends and amplitudes over the three largest ocean basins (Atlantic, Pacific and Indian Ocean, boundaries depicted in figure 1). Not surprising, the terrestrial hydrological cycle trend is negative for each basin but for the Atlantic Ocean it is about four times smaller compared to the Pacific and Indian ocean and about 70% smaller compared to the global mean hydrological sea level trend. The sea level trends in the Pacific and Indian ocean are 23% and 17% larger than the global mean. These relations are quite robust against using different setups in the inversion. Thus, although the total terrestrial hydrological cycle trends differ depending on the inversion setup, the spatial distribution is similar. The annual amplitude is found largest for the Indian Ocean, about 14% higher than the amplitude of the global mean hydrological sea level amplitude. For the Pacific Ocean the annual amplitude is only slightly larger (5%) than the global mean, whereas for the Atlantic Ocean the amplitude is about 16% smaller.

## 5. Conclusions

Using GRACE and Jason-1 data from the time period of August 2002 to July 2009 in an inverse fingerprint method, we find that land water storage change from the world's 33 largest hydrological basins contributes to global sea level change by $-0.20 \pm 0.04$ mm/yr with an annual amplitude of $6.6 \pm 0.5$ mm. To study the effect of using different methods, we apply our inversion method to GRACE data only and compare the results to the trends and amplitudes derived from GRACE with a basin averaging method. While we find considerable differences between the methods for individual catchments (up to 180%), results are quite robust in terms of global and regional sea level change. The major differences occur in North America and Eurasia, which we believe is due to GIA and glacier melting effects treated differently in the methods. In addition, in the fingerprint inversion, we do not need to filter the GRACE data and rescale the mass change estimates as we do in the basin averaging approach.

We have investigated the sensitivity of the fingerprint inversion method with respect to the data set (GRACE, GRACE and Jason-1), to the choice of the a-priori fingerprint mass distribution (uniform, leading EOFs from model) and to the treatment of GIA (fixed a-priori or scaled by estimated factor). Depending on the chosen setup, the total terrestrial hydrological cycle trend varies in a range of $21.6 \pm 14.8$ Gt/yr to $76.8 \pm 14.0$ Gt/yr, however, the seasonal amplitude variations are only small. Furthermore, the estimated total terrestrial hydrological cycle trend strongly depends on the time period considered, which is due to large interannual and decadal hydrological variations.

The spatial distribution of trend and annual amplitude for the sea level change due to terrestrial hydrological cycle mass changes is fairly robust with respect to different inversion setups. It displays a sea level rise around South America (max. 0.9 mm/yr) and West Africa (max. 0.4 mm/yr), and a sea level fall around North America (min. $-2.0$ mm/yr) and Australia (min. $-0.9$ mm/yr).

The inversion results indicate that they may be useful in improving the WGHM model in terms of seasonal amplitude and trend. Whereas in earlier model-based studies [*Milly et al.*, 2003; *Ngo-Duc et al.*, 2005] the contribution of terrestrial hydrological cycle mass changes to global mean sea level change was assumed to be slightly positive, in more recent studies based on GRACE data [*Llovel et al.*, 2010; *Riva et al.*, 2010] it was rather found to be negative in the same order of magnitude. This might be due to the different time frames considered. In this study we also find a small negative contribution of terrestrial hydrological cycle mass changes to global mean sea level change. Our estimate of $-0.20 \pm 0.04$ mm/yr agrees well with the result of *Llovel et al.* [2010] ($-0.22 \pm 0.05$ mm/yr), who used the same time period and the same hydrological basins. When we analyse the same time period that *Riva et al.* [2010] chose, i.e. January 2003 to December 2009, we obtain a terrestrial hydrological cycle-driven global mean sea level change of $-0.24 \pm 0.04$ which is also within the error bounds of the value of *Riva et al.* [2010] ($-0.1 \pm 0.3$ mm/yr). Not surprisingly, we also find the hydrological cycle-driven regional sea level change to be dominant in the coastal areas. Our spatial pattern of regional sea level trend is similar to the one of *Riva et al.* [2010], but the strong positive sea level trend these authors found for most of Northern Eurasia is much smaller in our results, which might be due to a different GIA model. The pattern of annual amplitude is quite close to the sea level amplitude pattern *Wouters et al.* [2011] derive from GRACE for continental water mass changes by solving the 'sea level equation'. However, as *Wouters et al.* [2011] consider mass changes from the whole land surface (not only from 33 hydrological basins) they find a larger global ocean mean amplitude of $9.4 \pm 0.6$ mm and (due to not excluding glaciers) lower amplitudes in the high latitudes compared to our results.

Future work will address improving our data base of a priori mass patterns we use in the inversion. The world's largest hydrological basins, in terms of surface area, are not necessarily those basins that contribute most to the terrestrial hydrological cycle trend and amplitude. By choosing other and possibly more hydrological basins, our estimate may become more robust. Furthermore, we plan to use more than one pattern for the GIA in order to adjust different regions of past glaciation (Laurentide, Fennoscandia,...) independently within the inversion. This requires a tradeoff since similar (in particular neighboring) patterns render the inversion unstable. Therefore, introducing formal constraints might be necessary. In addition, deep-ocean steric fingerprints from ocean circulation models could further help to explain observed sea level change.

## Appendix A: Calculation of sea level fingerprints

### A1. Sea level equation

The sea level fingerprints for the mass contributors to global mean sea level change are obtained in this study by solving the sea level equation [*Farrell and Clark*, 1976], which links the sea level change $\delta s(\lambda, \theta, t)$ at a location with longitude $\lambda$ and colatitude $\theta$ at a time $t$ with a continental mass load $\delta h(\lambda', \theta', t)$, expressed in equivalent water heights

$$\delta s(\lambda, \theta, t) = O(\lambda, \theta) \int_\Omega G^L_{N-U} \left(\delta s(\lambda', \theta', t) + \delta h(\lambda', \theta', t)\right) d\omega + \int_\Omega G^T_{N-U} \delta\Lambda(\delta s, \delta h) d\omega + \frac{\Delta V}{g}. \quad \text{(A1)}$$

Within Eq. (A1) we consider (a) gravitational effects of the mass load (b) gravitational effects of the sea level itself and (c) changes of the rotational potential $\delta\Lambda$ due to the changed surface loading distribution. The Green's functions $G^L_{N-U}$ and $G^T_{N-U}$ describe the elastic response of the Earth to a point-like, impulse mass load (index $L$) and to general potential forcing (index $T$), respectively. They are given in terms of the difference between the geoid $N$ and the associated uplift $U$ [*Farrell*, 1972]. As $\delta s(\lambda, \theta, t)$ is only defined over the ocean, the ocean function $O(\lambda, \theta)$ is applied, which is zero over land and unity over the ocean. The term $\frac{\Delta V}{g}$ is a uniform shift of the geoid, added to conserve the mass of the global surface loading distribution $\delta T$

$$\int_\Omega \delta T(\lambda', \theta', t) d\omega = \int_\Omega \left(\delta s(\lambda', \theta', t) + \delta h(\lambda', \theta', t)\right) d\omega = 0. \quad \text{(A2)}$$

In the spectral domain, and using linearized Euler equations, we can express Eq.(A1) in a matrix notation

$$\tilde{S} = \mathbf{G}^L_{N-U}(\mathbf{O}\tilde{S} + \overrightarrow{H}) + \mathbf{G}^T_{N-U}\mathbf{\Xi}(\mathbf{O}\tilde{S} + \overrightarrow{H}). \quad \text{(A3)}$$

Eq. (A3) is linear in $\tilde{S}$ and can thus be solved by inversion:

$$\tilde{S} = (\mathbf{1} - \mathbf{G}^L_{N-U}\mathbf{O} - \mathbf{G}^T_{N-U}\mathbf{\Xi}\mathbf{O})^{-1}(\mathbf{G}^L_{N-U} + \mathbf{G}^T_{N-U}\mathbf{\Xi})\overrightarrow{H}. \quad \text{(A4)}$$

The vectors $\tilde{S}$ and $\overrightarrow{H}$ contain the (stacked) spherical harmonic coefficients of the sea level and the load distribution; $\mathbf{G}^L_{N-U}$ and $\mathbf{G}^T_{N-U}$ are the matrix representations of the Green's Functions $G^L_{N-U}$ and $G^T_{N-U}$. Multiplication with matrix $\mathbf{O}$ represents the spectral convolution with the ocean function. Due to the relatively short time period of seven years considered in this study $\mathbf{O}$ is assumed to be time-independent. The matrix $\mathbf{\Xi}$ converts the changes of the surface loading into rotational potential changes.

The vector $\tilde{S}$ is the quasi-spectral sea level and represents an equipotential surface shifted by a uniform constant. To obtain the sea level $\overrightarrow{S}$ which is zero over land (and not an equipotential surface), the ocean function has to be applied

$$\overrightarrow{S} = \mathbf{O}\tilde{S}. \tag{A5}$$

The Green's functions $\mathbf{G}^L_{N-U}$ and $\mathbf{G}^T_{N-U}$ are only defined for degrees larger than zero. Thus we augment the spectral representation of the sea level equation by a degree zero term which ensures mass conservation according to

$$\overrightarrow{S}_{00} = -\overrightarrow{H}_{00} = \sum_{n=0}^{n_{max}} \sum_{m=-n}^{n} O_{nm}\tilde{S}_{nm}. \tag{A6}$$

## A2. Green's functions

Assuming a spherical, non-rotating, elastic and isotropic Earth, the matrices $\mathbf{G}^L_{N-U}$ and $\mathbf{G}^T_{N-U}$ are diagonal and depend on the load Love numbers $h'_n$, $k'_n$ and body Love numbers $h_n$, $k_n$, respectively:

$$\mathbf{G}^L_{N-U} = diag\left\{\frac{3\rho_w}{(2n+1)\rho_e}(1 + k'_n - h'_n)\right\}, \quad n > 0, \tag{A7}$$

with $\rho_w$ and $\rho_e$ being the density of sea water and the mean density of the solid Earth, and

$$\mathbf{G}^T_{N-U} = diag\left\{\frac{1}{g}(1+k_n-h_n)\right\}, \quad n>0. \tag{A8}$$

### A3. Rotational feedback

The matrix $\mathbf{\Xi}$ for mapping surface loading changes to rotational potential can be splitted into a product of three (sparse) matrices

$$\mathbf{\Xi} = \underset{\Lambda\leftarrow m}{\mathbf{\Phi}} \quad \underset{m\leftarrow J}{\mathbf{\Gamma}} \quad \underset{J\leftarrow T}{\mathbf{\Psi}}. \tag{A9}$$

The matrix $\underset{J\leftarrow T}{\mathbf{\Psi}}$ converts the degree 2 surface loading coefficients $T_{2m}$ to the corresponding moments of inertia $J_i^R$ of the rigid Earth, neglecting higher order moments of inertia [*Milne and Mitrovica*, 1998]

$$\begin{pmatrix} \delta J_1^R \\ \delta J_2^R \\ \delta J_3^R \end{pmatrix} = \pi a^4 \rho_w \begin{pmatrix} 0 & 0 & -\frac{4}{5}\sqrt{\frac{10}{6}} & 0 \\ 0 & 0 & 0 - \frac{4}{5}\sqrt{\frac{10}{6}} & \\ \frac{8}{3} & -\frac{8}{3\sqrt{5}} & 0 & 0 \end{pmatrix} \begin{pmatrix} T_{00} \\ T_{20} \\ T_{2,1} \\ T_{2,-1} \end{pmatrix}. \tag{A10}$$

Here, $a$ is the mean radius of the Earth. Changes in the moments of inertia $J_i^R$ are linked to the polar motion $m$ with the matrix $\underset{m\leftarrow J}{\mathbf{\Gamma}}$ [*Mitrovica et al.*, 2005]

$$\begin{pmatrix} m_1 \\ m_2 \\ m_3 \end{pmatrix} = \begin{pmatrix} \Omega\frac{1+k_2'}{A\sigma_0} & 0 & 0 \\ 0 & \Omega\frac{1+k_2'}{A\sigma_0} & 0 \\ 0 & 0 & -\frac{1+k_2'}{C} \end{pmatrix} \begin{pmatrix} \delta J_1^R \\ \delta J_2^R \\ \delta J_3^R \end{pmatrix}, \tag{A11}$$

where $\Omega$ is the mean angular frequency of the Earth, $A$ and $C$ are the Earth's principal moments of inertia and $\sigma_0$ is the Chandler frequency. Finally, a change of the polar motion has a feedback on the rotational potential $\Lambda$, expressed with the matrix $\underset{\Lambda\leftarrow m}{\mathbf{\Phi}}$ [*Milne and Mitrovica*, 1998]

$$\begin{pmatrix} \Lambda_{00} \\ \Lambda_{20} \\ \Lambda_{2,1} \\ \Lambda_{2,-1} \end{pmatrix} = (a\Omega)^2 \begin{pmatrix} 0 & 0 & \frac{2}{3} \\ 0 & 0 & -\frac{2}{3\sqrt{(5)}} \\ -\frac{1}{\sqrt{15}} & 0 & 0 \\ 0 & -\frac{1}{\sqrt{15}} & 0 \end{pmatrix} \begin{pmatrix} m_1 \\ m_2 \\ m_3 \end{pmatrix}. \tag{A12}$$

**Acknowledgments.** We thank two anonymous reviewers for their instructive and very useful comments. The authors acknowledge support provided by the German Research Foundation (DFG) under grant KU 1207/9-2 within the German priority program SPP 1257: Mass Transport and Mass Distribution in the System Earth.

## References

Adam, L., P. Döll, C. Prigent, and F. Papa (2010), Global-scale analysis of satellite-derived time series of naturally inundated areas as a basis for floodplain modeling, *Ad. Geo.*, *27*, 45–50, doi:10.5194/adgeo-27-45-2010.

aus der Beek, T., L. Menzel, R. Rietbroek, L. Fenoglio-Marc, S. Grayek, M. Becker, J. Kusche, and E. Stanev (2011), Modeling the water resources of the Black and Mediterranean Sea river basins and their impact on regional mass changes, *J. Geodyn.*, *59-60*, 157–167, doi:10.1016/j.jog.2011.11.011.

Baur, O., M. Kuhn, and W. E. Featherstone (2009), GRACE-derived ice-mass variations over Greenland by accounting for leakage effects, *J. Geophys. Res. (Solid Earth)*, *114* (B13), 6407–+, doi:10.1029/2008JB006239.

Bindoff, N. L., J. Willebrand, V. Artale, A. Cazenave, J. Gregory, S. Gulev, and K. Hanawa (2007), Observations: oceanic climate change and sea level, in *Climate Change 2007: The Physical Science Basis: Contribution of Working Group I to the Fourth Assessment Report of the Intergovernmental Panel on Climate Change*, edited by S. Solomon, D. Qin, M. Manning, Z. Chen, M. Marquis, K. Averyt, M. Tignor, and H. Miller, pp. 385–433, Cambridge University Press.

Blewitt, G., and P. Clarke (2003), Inversion of Earth's changing shape to weigh sea level in static equilibrium with surface mass redistribution, *J. Geophys. Res. (Solid Earth)*, *108*, 2311, doi:10.1029/2002JB002290.

Brunnabend, S.-E., J. Schröter, R. Timmermann, R. Rietbroek, and J. Kusche (2011), Modeled steric and mass-driven sea level change caused by greenland ice sheet melting, *J. Geodyn.*, doi:10.1016/j.jog.2011.06.001.

Cazenave, A., and W. Llovel (2010), Contemporary sea level rise, *Annu. Rev. Mar. Sci.*, *2* (1), 145–173, doi:10.1146/annurev-marine-120308-081105.

Chambers, D. P., and J. Schröter (2011), Measuring ocean mass variability from satellite gravimetry, *J. Geodyn.*, *52* (5), 333 – 343, doi:10.1016/j.jog.2011.04.004.

Chambers, D. P., J. C. Ries, and T. J. Urban (2003), Calibration and verification of Jason-1 using global along-track residuals with TOPEX special issue: Jason-1 calibration/validation, *Mar. Geod.*, *26* (3), 305–317, doi:10.1080/714044523.

Chao, B., Y. H. Wu, and Y. S. Li (2008), Impact of artificial reservoir water impoundment on global sea level, *Science*, *320*, 212–, doi:10.1126/science.1154580.

Cheng, M., and B. D. Tapley (2004), Variations in the Earth's oblateness during the past 28 years, *J. Geophys. Res. (Solid Earth)*, *109*(18), 9402–+, doi:10.1029/2004JB003028.

Cogley, J. G. (2009), Geodetic and direct mass-balance measurements: comparison and joint analysis, *Ann. Glaciol.*, pp. 96–100, doi:10.3189/172756409787769744.

Dahle, C., F. Flechtner, J. Kusche, and R. Rietbroek (2008), GFZ EIGEN-GRACE05S (RL04) Weekly Gravity Field Time Series, Proceedings of the 2008 GRACE Science Team Meeting, San Francisco, http://www.csr.utexas.edu/grace/GSTM.

Dahlen, F. A. (1976), The passive influence of the oceans upon the rotation of the Earth, *Geophys. J. Roy. Astr. S.*, *46*(2), 363–406, doi:10.1111/j.1365-246X.1976.tb04163.x.

Döll, P., F. Kaspar, and B. Lehner (2003), A global hydrological model for deriving water availability indicators: model tuning and validation, *J. Hydrol.*, *270*(1-2), 105–134, doi:10.1016/S0022-1694(02)00283-4.

Döll, P., H. Hoffmann-Dobrev, F. T. Portmann, S. Siebert, A. Eicker, M. Rodell, G. Strassberg, and B. R. Scanlon (2011), Impact of water withdrawals from groundwater and surface water on continental water storage variations, *J. Geodyn.*, *59-60*, 143–156, doi: 10.1016/j.jog.2011.05.001.

Ewert, H., A. Groh, and R. Dietrich (2012), Volume and mass changes of the Greenland ice sheet inferred from ICESat and GRACE, *J. Geodyn.*, *59 - 60*(0), 111 – 123, doi: 10.1016/j.jog.2011.06.003.

Farrell, W. E. (1972), Deformation of the Earth by Surface Loads, *Rev. Geophys. Space Phys.*, *10*, 761, doi:10.1029/RG010i003p00761.

Farrell, W. E., and J. A. Clark (1976), On postglacial sea level, *Geophys. J. Roy. Astr. S.*, *46*(3), 647–667, doi:10.1111/j.1365-246X.1976.tb01252.x.

Fenoglio-Marc, L., R. Rietbroek, S. Grayek, M. Becker, J. Kusche, and E. Stanev (2012), Water mass variation in the Mediterranean and Black Seas, *J. Geodyn.*, *59 - 60*(0), 168 – 182, doi:10.1016/j.jog.2012.04.001.

Fiedler, J. W., and C. P. Conrad (2010), Spatial variability of sea level rise due to water impoundment behind dams, *Geophys. Res. Let.*, *37*(12), L12,603, doi: 10.1029/2010GL043462.

Fiedler, K., and P. Döll (2007), Global modelling of continental water storage changes: sensitivity to different climate data sets, *Ad. Geo.*, *11*, 63–68, doi:10.5194/adgeo-11-63-2007.

Flechtner, F. (2007), GFZ Level-2 processing standards document for level-2 product release 0004, GRACE 327-743, Rev. 1.0.

Forootan, E., J. Awange, J. Kusche, B. Heck, and A. Eicker (2012), Independent patterns of water mass anomalies over Australia from satellite data and models, *Remote Sens. Environ.*, *124*(0), 427 – 443, doi:10.1016/j.rse.2012.05.023.

Guo, J., Z. Huang, C. Shum, and W. van der Wal (2012), Comparisons among contemporary glacial isostatic adjustment models, *J. Geodyn.*, doi:10.1016/j.jog.2012.03.011.

Horwath, M., and R. Dietrich (2009), Signal and error in mass change inferences from GRACE: the case of Antarctica, *Geophys. J. Int.*, *177*(3), 849–864, doi:10.1111/j.1365-246X.2009.04139.x.

Hosoda, S., T. Ohira, and T. A. Nakamura (2008), Monthly mean dataset of global oceanic temperature and salinity derived from Argo float observations, *JAMSTEC Report of Research and Development*, *8*, 47–59.

Jacob, T., J. Wahr, W. T. Pfeffer, and S. Swenson (2012), Recent contributions of glaciers and ice caps to sea level rise, *Nature*, *482*, 514–518, doi:10.1038/nature10847.

Klees, R., A. Revtova, B. C. Gunter, P. Ditmar, E. Oudman, H. C. Winsemius, and H. H. G. Savenije (2008), The design of an optimal filter for monthly GRACE gravity models, *Geophys. J. Int.*, *175*, 417–432+, doi:10.1111/j.1365-246X.2008.03922.x.

Klemann, V., and Z. Martinec (2009), Contribution of glacial-isostatic adjustment to the geocenter motion., *Tectonophysics*, *511*, 99–108, doi:10.1016/j.tecto.2009.08.031.

Konikow, L. F. (2011), Contribution of global groundwater depletion since 1900 to sea-level rise, *Geophys. Res. Let.*, *38*(17), L17,401+, doi:10.1029/2011GL048604.

Kusche, J. (2007), Approximate decorrelation and non-isotropic smoothing of time-variable GRACE-type gravity field models, *J. Geodesy*, *81*(11), 733–749, doi:10.1007/s00190-007-0143-3.

Leuliette, E. W., and L. Miller (2009), Closing the sea level rise budget with altimetry, Argo, and GRACE, *Geophys. Res. Let.*, *36*(4), –04,608, doi:10.1029/2008GL036010.

Llovel, W., M. Becker, A. Cazenave, J. Cretaux, and G. Ramillien (2010), Global land water storage change from GRACE over 2002-2009; Inference on sea level, *C. R. Geosci.*, *342*(3), 179–188, doi:10.1016/j.crte.2009.12.004.

Longuevergne, L., B. R. Scanlon, and C. R. Wilson (2010), GRACE hydrological estimates for small basins: Evaluating processing approaches on the High Plains Aquifer, *Water Resour. Res.*, *46*(W11517), 647–667, doi:10.1029/2009WR008564.

Milly, P., and A. Shmakin (2002), Global modeling of land water and energy balances. Part II: Land-characteristic contributions to spatial variability, *J. Hydrometeorol.*, *3*(3), 301–310, doi:10.1175/1525-7541(2002)003<0301:GMOLWA>2.0.CO;2.

Milly, P. C. D., A. Cazenave, and C. Gennero (2003), Contribution of climate-driven change in continental water storage to recent sea-level rise, *P. Natl. Acad. Sci. USA*, *100*(23), 13,158–13,161, doi:10.1073/pnas.2134014100.

Milne, G. A., and J. Mitrovica (1998), Postglacial sea-level change on a rotating Earth, *Geophys. J. Int.*, *133*, 1–19, doi:10.1046/j.1365-246X.1998.1331528.x.

Milne, G. A., W. R. Gehrels, C. W. Hughes, and M. Tamisiea (2009), Identifying the causes of sea-level change, *Nat. Geosci.*, *2*, 471–478, doi:10.1038/ngeo544.

Mitrovica, J. X., J. Wahr, I. Matsuyama, and A. Paulson (2005), The rotational stability of an ice-age Earth, *Geophys. J. Int.*, *161*(2), 491–506, doi:10.1111/j.1365-246X.2005.02609.x.

Nerem, R. S., D. Chambers, C. Choe, and G. T. Mitchum (2010), Estimating mean sea level change from the TOPEX and Jason altimeter missions, *Mar. Geod.*, *33*, 435, doi: 10.1080/01490419.2010.491031.

Ngo-Duc, T., K. Laval, J. Polcher, A. Lombard, and A. Cazenave (2005), Effects of land water storage on global mean sea level over the past half century, *Geophys. Res. Let.*, *32*(9), L09,704, doi:10.1029/2005GL022719.

Nicholls, R. J., and A. Cazenave (2010), Sea-level rise and its impact on coastal zones, *Science*, *328*, 1517 – 1520, doi:10.1126/science.1185782.

NSIDC (1999), Word Glacier inventory (updated 2009), World Glacier Monitoring Service and National Snow and Ice Data Center/World Data Center for Glaciology. Boulder, CO. Digital media, http://nsidc.org/data/docs/noaa/g01130_glacier_inventory.

Oki, T., and Y. C. Sud (1998), Design of total runoff integrating pathways (TRIP)–A global river channel network, *Earth Interact.*, *2*(1), 1.

Peixoto, J. P., and A. H. Oort (1992), *Physics of Climate.*, 520 pp., American Institute of Physics, New York, 520pp.

Peltier, W. R. (2004), Global Glacial Isostasy and the Surface of the Ice-Age Earth: The ICE-5G (VM2) Model and GRACE, *Annu. Rev. Earth Pl. Sc.*, *32*, 111–149, doi: 10.1146/annurev.earth.32.082503.144359.

Plag, H. P., and H. U. Jüttner (2001), Inversion of global tide gauge data for present-day ice load changes, *Mem. Natl. Inst. Polar Res. Spec. Issue*, *54*, 301–317.

Pokhrel, Y., N. Hanasaki, P. Yeh, T. Yamada, S. Kanae, and T. Oki (2012), Model estimates of sea-level change due to anthropogenic impacts on terrestrial water storage, *Nat. Geosci.*, doi:10.1038/ngeo1476.

Ramillien, G., S. Bouhours, A. Lombard, A. Cazenave, F. Flechtner, and R. Schmidt (2008), Land water storage contribution to sea level from GRACE geoid data over 2003-2006, *Global Planet. Change*, *60*(3), 381–392, doi:10.1016/j.gloplacha.2007.04.002.

Rietbroek, R., S.-E. Brunnabend, J. Kusche, and J. Schröter (2011), Resolving sea level contributions by identifying fingerprints in time-variable gravity and altimetry, *J. Geodyn.*, doi:10.1016/j.jog.2011.06.007.

Riva, R., J. Bamber, D. Lavallee, and B. Wouters (2010), Sea-level fingerprint of continental water and ice mass change from GRACE, *Geophys. Res. Let.*, *37*(19), doi: 10.1029/2010GL044770.

Rowlands, D. D., S. B. Luthcke, J. J. McCarthy, S. M. Klosko, D. S. Chinn, F. G. Lemoine, J. P. Boy, and T. J. Sabaka (2010), Global mass flux solutions from GRACE: A comparison of parameter estimation strategiesMass concentrations versus stokes coefficients, *J. Geophys. Res*, *115*(B1), B01,403+, doi:10.1029/2009JB006546.

Rudolf, B., and U. Schneider (2005), Calculation of gridded precipitation data for the global land-surface using in-situ gauge observations, *Proceedings of the 2nd Workshop of the International Precipitation Working Group IPWG*, pp. 231–247.

Schmidt, R., S. Petrovic, A. Güntner, F. Barthelmes, J. Wünsch, and J. Kusche (2008), Periodic components of water storage changes from GRACE and global hydrology models, *J. Geophys. Res. (Solid Earth)*, *113*, 08,419, doi:10.1029/2007JB005363.

Schrama, E., B. Wouters, and B. Vermeersen (2011), Present Day Regional Mass Loss of Greenland Observed with Satellite Gravimetry, *Surv. Geophys.*, *32*, 377–385, doi: 10.1007/s10712-011-9113-7.

Schwatke, C., W. Bosch, R. Savcenko, and D. Dettmering (2010), OpenADB: An open database for multi-mission altimetry, *EGU Geophysical research abstracts*, http://openadb.dgfi.badw.de.

Slangen, A., C. Katsman, R. van de Wal, L. Vermeersen, and R. Riva (2012), Towards regional projections of twenty-first century sea-level change based on ipcc sres scenarios, *Clim. Dynam.*, *38*, 1191–1209, doi:10.1007/s00382-011-1057-6.

Spada, G., and P. Stocchi (2007), SELEN: A Fortran 90 program for solving the "sea-level equation", *Comput. Geosci.*, *33*(4), 538–562, doi: http://dx.doi.org/10.1016/j.cageo.2006.08.006.

Swenson, S., and J. Wahr (2006), Post-processing removal of correlated errors in GRACE data, *Geophys. Res. Let.*, *33*, doi:10.1029/2005GL025285.

Velicogna, I. (2009), Increasing rates of ice mass loss from the Greenland and Antarctic ice sheets revealed by GRACE, *Geophys. Res. Let.*, *36*(19), L19,503+, doi: 10.1029/2009GL040222.

Velicogna, I., and J. M. Wahr (2006), Measurements of time-variable gravity show mass loss in Antarctica, *Science*, *311*, 1754–1756, doi:10.1126/science.1123785.

Vörösmarty, C. J., and D. Sahagian (2000), Anthropogenic disturbance of the terrestrial water cycle, *Bioscience*, *50*(9), 753–765, doi:10.1641/0006-3568(2000)050[0753:ADOTTW]2.0.CO;2.

Wada, Y., L. van Beek, F. Sperna Weiland, B. Chao, Y. H. Wu, and M. Bierkens (2012), Past and future contribution of global groundwater depletion to sea-level rise, *Geophys. Res. Let.*, *39*, doi:10.1029/2012GL051230.

Wahr, J., M. Molenaar, and F. Bryan (1998), Time variability of the Earth's gravity field: Hydrological and oceanic effects and their possible detection using GRACE, *J. Geophys. Res.*, *103*, 30,205–30,230, doi:10.1029/98JB02844.

Wang, H. S., P. Wu, and W. van der Wal (2008), Using postglacial sealevel, crustal velocities and gravity-rate-of-change to constrain the influence of thermal effects on mantle lateral heterogeneities, *J. Geodyn.*, *46*, 104–117.

Werth, S., and A. Güntner (2010), Calibration analysis for water storage variability of the global hydrological model WGHM, *Hydrol. Earth Syst. Sci.*, *14*, 59–78.

Wouters, B., R. E. M. Riva, D. A. Lavallée, and J. L. Bamber (2011), Seasonal variations in sea level induced by continental water mass: First results from GRACE, *Geophys. Res. Let.*, *38*, 3303–+, doi:10.1029/2010GL046128.

Wu, X., M. B. Heflin, H. Schotman, B. L. A. Vermeersen, D. Dong, R. S. Gross, E. R. Ivins, A. W. Moore, and S. E. Owen (2010), Simultaneous estimation of global present-day water transport and glacial isostatic adjustment, *Nat. Geosci.*, *3*(9), 642, doi:10.1038/ngeo938.

Wu, X., J. Ray, and T. van Dam (2012), Geocenter motion and its geodetic and geophysical implications, *J. Geodyn.*, *58*, 44–61, doi:10.1016/j.jog.2012.01.007.

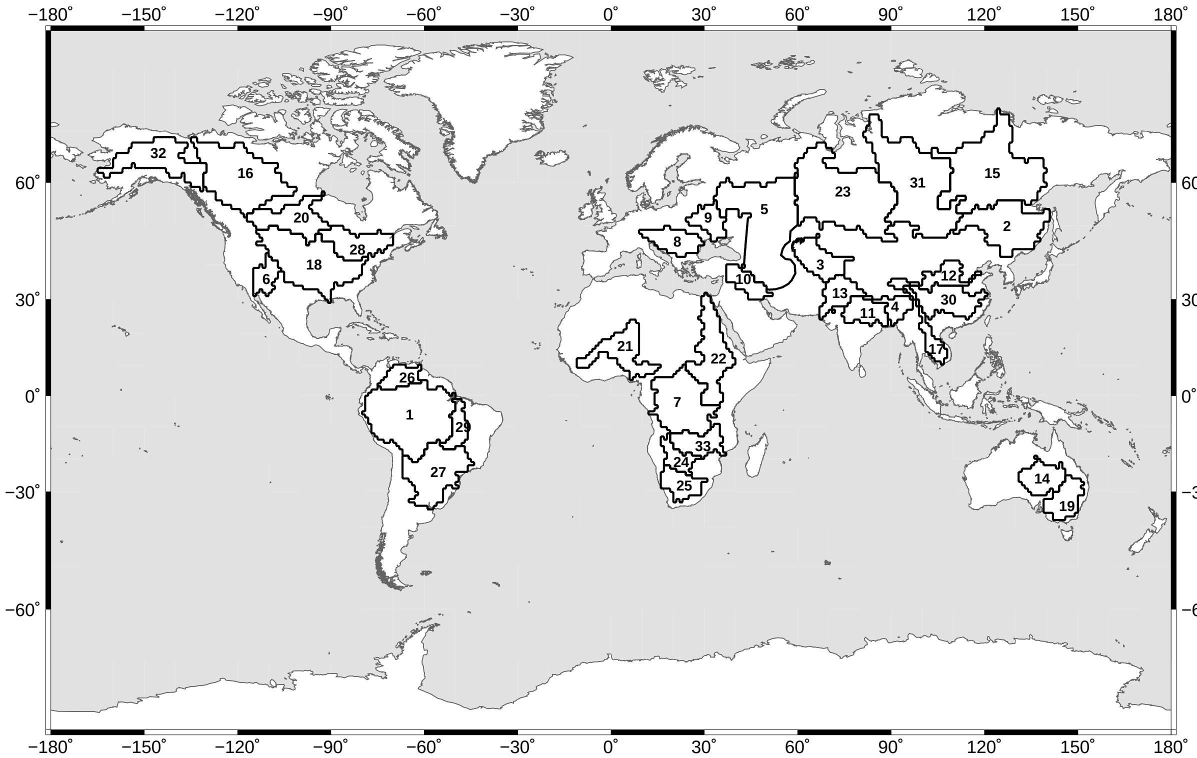


Figure 1: Outlines of the 33 world's largest river basins considered in this study (black lines). The outlines of the three biggest ocean basins (used in section 4.2) are depicted in dark grey (Indian Ocean), middle grey (Atlantic Ocean) and light grey (Pacific Ocean).

Table 1: Trend of mass variations [Gt/yr] from 33 basins for 08/2002 to 07/2009.[a]

| No. | Name | **BasAv** | **InvGR** | **Inv** | **InvEOF** | **WGHM** |
|---|---|---|---|---|---|---|
| 1 | **Amazon** | 101.9 | 82.7 | 67.2 | 67.0 | 90.4 |
| 2 | **Amur** | -5.6 | -7.6 | -6.2 | -1.7 | 2.7 |
| 3 | **Aral** | -14.5 | -1.1 | -3.3 | 3.4 | -2.0 |
| 4 | **Brahmaputra** | -12.4 | 5.7 | 4.8 | 3.4 | 1.1 |
| 5 | **Caspian-Volga** | -24.9 | -18.0 | -18.3 | 1.4 | -17.1 |
| 6 | **Colorado** | -2.0 | -13.4 | -14.5 | -13.9 | -1.4 |
| 7 | **Congo** | 2.8 | 19.2 | 13.6 | 10.7 | 40.1 |
| 8 | **Danube** | 2.7 | -3.8 | -6.2 | -5.7 | -0.7 |
| 9 | **Dnepr** | -1.1 | 5.7 | 6.1 | 2.8 | -1.1 |
| 10 | **Euphrates** | -19.9 | -19.4 | -20.5 | -21.0 | -6.0 |
| 11 | **Ganges** | -22.6 | -16.7 | -15.9 | -18.1 | -16.0 |
| 12 | **Huanghe** | -3.2 | -14.8 | -13.8 | -15.5 | -3.4 |
| 13 | **Indus** | -17.3 | -1.8 | -2.2 | -5.7 | 2.1 |
| 14 | **Lake-Eyre** | -6.6 | -7.1 | -7.7 | -5.4 | 0.4 |
| 15 | **Lena** | 19.9 | 24.3 | 25.1 | 10.6 | 11.1 |
| 16 | **Mackenzie** | -3.0 | -18.5 | -18.9 | 1.3 | 7.6 |
| 17 | **Mekong** | 0.0 | -9.9 | -8.0 | -5.3 | 0.6 |
| 18 | **Mississippi** | 3.0 | -14.6 | -17.6 | -19.1 | 5.9 |
| 19 | **Murray** | -7.3 | -8.5 | -9.8 | -12.2 | 0.1 |
| 20 | **Nelson** | -8.4 | -1.9 | -2.2 | -6.7 | 15.0 |
| 21 | **Niger** | 10.3 | 25.7 | 20.1 | 24.5 | 1.7 |
| 22 | **Nile** | 25.8 | 26.9 | 21.6 | 24.8 | 8.4 |
| 23 | **Ob** | -1.8 | 18.1 | 17.3 | 9.9 | 3.8 |
| 24 | **Okavango** | 14.0 | 21.9 | 19.9 | 17.3 | 5.6 |
| 25 | **Orange** | 2.9 | -8.0 | -9.8 | -6.0 | 0.9 |
| 26 | **Orinoco** | 16.0 | 31.2 | 28.0 | 21.7 | 10.2 |
| 27 | **Parana** | -4.8 | -4.3 | -14.9 | 12.3 | -8.9 |
| 28 | **St-Lawrence** | 4.4 | 4.4 | 5.6 | 8.1 | 8.7 |
| 29 | **Tocantins** | 4.8 | 7.0 | 6.4 | 9.2 | -0.4 |
| 30 | **Yangtze** | 13.8 | 19.5 | 21.1 | 17.6 | -4.3 |
| 31 | **Yenisei** | 23.5 | -0.1 | 1.3 | 13.4 | 6.4 |
| 32 | **Yukon** | -21.0 | -56.8 | -56.3 | -61.0 | 1.5 |
| 33 | **Zambezi** | 20.4 | 10.7 | 9.6 | 12.4 | 2.8 |
| | **TOTAL** | 89.7±16.4 | 76.8±1.4 | 21.6±1.5 | 74.7±1.4 | 165.7 |
| | **Mean Rel. Diff.** [%] | | 62.5 | 63.1 | 70.8 | 79.4 |
| | **Rel.Diff. Total** [%] | | 14.4 | 75.9 | 16.7 | 45.9 |

[a] *BasAv* indicates the results obtained with a GRACE basin averaging method. *InvGR* indicates the results obtained with the fingerprint inversion method, using only GRACE data (GIA scale fixed to 1.0). *Inv* indicates the results of the multisensor fingerprint inversion using GRACE and Jason-1 data (GIA scale fixed to 1.0). *InvEOF* is our 'best estimate' from the fingerprint inversion using GRACE and Jason-1 and EOF WGHM fingerprints (two for Amazon basin, one for the others) for the terrestrial hydrological changes (GIA scale co-estimated). *WGHM* are the trends obtained from the WGHM.

Table 2: Annual amplitude of mass variations [Gt] from 33 basins for 08/2002 to 07/2009.[a]

| No. | Name | **BasAv** | **InvGR** | **Inv** | **InvEOF** | **WGHM** |
|---:|---|---:|---:|---:|---:|---:|
| 1 | **Amazon** | 1171.0 (4.4) | 1312.5 (4.8) | 1306.1 (4.7) | 1207.0 (4.8) | 520.1 (3.7) |
| 2 | **Amur** | 48.6 (4.6) | 34.9 (4.2) | 30.0 (4.2) | 1.9 (6.2) | 14.8 (0.4) |
| 3 | **Aral** | 91.9 (4.1) | 77.9 (5.6) | 79.2 (5.4) | 77.4 (5.1) | 27.3 (2.9) |
| 4 | **Brahmaputra** | 126.5 (8.4) | 266.5 (8.8) | 261.5 (8.8) | 240.4 (9.0) | 65.0 (8.5) |
| 5 | **Caspian-Volga** | 228.1 (4.0) | 268.5 (4.3) | 267.3 (4.2) | 236.4 (3.7) | 198.8 (2.5) |
| 6 | **Colorado** | 35.8 (3.2) | 29.8 (2.8) | 37.4 (2.3) | 50.3 (3.1) | 8.0 (1.8) |
| 7 | **Congo** | 171.8 (2.3) | 163.7 (2.6) | 201.6 (2.5) | 287.7 (3.5) | 88.1 (2.0) |
| 8 | **Danube** | 62.8 (3.3) | 65.5 (3.0) | 64.5 (3.0) | 80.1 (2.6) | 56.8 (2.4) |
| 9 | **Dnepr** | 52.9 (3.5) | 120.5 (3.7) | 115.6 (3.7) | 85.9 (4.0) | 38.8 (2.3) |
| 10 | **Euphrates** | 71.2 (3.9) | 164.6 (4.0) | 167.4 (4.0) | 156.8 (4.1) | 24.6 (2.5) |
| 11 | **Ganges** | 172.7 (9.5) | 282.4 (10.6) | 280.3 (10.6) | 210.7 (10.5) | 91.4 (9.0) |
| 12 | **Huanghe** | 18.5 (10.9) | 74.5 (1.3) | 71.6 (1.3) | 49.9 (1.5) | 13.3 (9.1) |
| 13 | **Indus** | 29.0 (4.1) | 55.6 (7.2) | 52.8 (7.1) | 42.8 (5.7) | 10.6 (3.8) |
| 14 | **Lake-Eyre** | 5.7 (11.2 | 51.8 (4.0) | 64.5 (3.8) | 88.1 (4.1) | 4.1 (2.1) |
| 15 | **Lena** | 117.2 (3.3) | 203.1 (3.6) | 199.2 (3.5) | 160.5 (3.6) | 89.2 (2.7) |
| 16 | **Mackenzie** | 109.1 (3.5) | 78.7 (3.7) | 80.5 (3.5) | 49.3 (3.2) | 86.7 (2.9) |
| 17 | **Mekong** | 226.8 (9.5) | 452.8 (10.6) | 444.0 (10.6) | 358.9 (10.7) | 87.7 (8.8) |
| 18 | **Mississippi** | 207.6 (3.9) | 301.5 (3.9) | 306.1 (3.7) | 273.5 (3.6) | 147.5 (2.7) |
| 19 | **Murray** | 38.6 (9.3) | 82.4 (7.4) | 67.4 (7.1) | 52.0 (7.4) | 11.5 (8.8) |
| 20 | **Nelson** | 45.4 (4.2) | 53.6 (3.5) | 56.1 (3.3) | 85.0 (3.5) | 37.0 (2.6) |
| 21 | **Niger** | 221.8 (9.5) | 383.9 (10.0) | 368.4 (10.2) | 430.5 (10.4) | 86.2 (9.3) |
| 22 | **Nile**) | 215.1 (9.7) | 247.9 (10.3) | 241.5 (10.5) | 192.7 (10.4) | 81.2 (8.8) |
| 23 | **Ob**) | 200.8 (3.7) | 219.1 (3.9) | 224.8 (3.8) | 159.6 (4.0) | 176.9 (2.7) |
| 24 | **Okavango** | 62.6 (3.7) | 19.9 (10.3) | 19.2 (11.5) | 23.8 (0.3) | 18.2 (2.5) |
| 25 | **Orange** | 12.7 (4.7) | 46.1 (7.8) | 20.1 (7.5) | 18.8 (8.6) | 4.5 (2.1) |
| 26 | **Orinoco** | 211.0 (8.7) | 295.3 (9.3) | 293.0 (9.4) | 195.0 (10.0) | 99.2 (8.8) |
| 27 | **Parana** | 162.4 (3.7) | 137.5 (4.5) | 151.5 (4.0) | 197.6 (4.0) | 93.7 (2.9) |
| 28 | **St-Lawrence** | 76.0 (3.6) | 116.3 (2.9) | 117.3 (2.8) | 110.6 (2.8) | 89.6 (2.8) |
| 29 | **Tocantins** | 326.8 (3.9) | 396.0 (4.4) | 396.5 (4.3) | 371.7 (4.7) | 117.1 (3.5) |
| 30 | **Yangtze** | 95.3 (7.8) | 102.6 (8.7) | 107.3 (8.7) | 103.3 (8.8) | 80.8 (8.1) |
| 31 | **Yenisei** | 153.5 (3.0) | 144.6 (3.5) | 137.7 (3.5) | 154.7 (3.7) | 129.1 (2.8) |
| 32 | **Yukon** | 88.9 (3.2) | 120.9 (3.5) | 118.2 (3.5) | 91.3 (3.7) | 47.5 (2.8) |
| 33 | **Zambezi** | 239.9 (3.7) | 459.9 (4.3) | 468.8 (4.2) | 357.4 (4.2) | 71.2 (2.9) |
| Amp. | **TOTAL** | 2478.1±214.1 | 2375.6±18.0 | 2468.7±22.5 | 2442.6±20.4 | 1406.8 |
| Pha. | **TOTAL** | 4.20±0.04 | 4.25±0.01 | 4.14±0.01 | 4.14±0.01 | 3.02 |
| Amp. | **Mean Diff.** [%] | | 33.9 | 32.5 | 32.1 | 44.5 |
| Amp. | **Diff. Total** [%] | | 4.1 | 0.4 | 1.4 | 43.2 |
| Pha. | **RMSE** [mn] | | 0.29 | 0.27 | 0.26 | 0.27 |
| Pha. | **Diff. Total** [mn] | | 0.05 | -0.05 | -0.06 | -1.17 |

[a] The numbers in brackets give the time in the year (in months) when the maximum of the annual variation is reached (phase).

Table 3: Trend of terrestrial hydrological mass variations [Gt/yr] accumulated over the continents for 08/2002 to 07/2009.

| | **BasAv** | **InvGR** | **Inv** | **InvEOF** | **WGHM** |
|---|---|---|---|---|---|
| **South America** | 117.8 | 116.5 | 86.7 | 110.2 | 91.3 |
| **North America** | -27.0 | -100.8 | -104.0 | -91.3 | 37.2 |
| **Africa** | 76.2 | 96.4 | 75.0 | 83.6 | 59.5 |
| **Eurasia** | -63.3 | -19.8 | -18.6 | -10.3 | -22.7 |
| **Australia** | -14.0 | -15.5 | -17.5 | -17.6 | 0.5 |
| **Mean Rel.Diff** [%] | | 34.8 | 38.6 | 38.0 | 76.9 |

Table 4: global mean sea level contributions, estimated from GRACE and Jason-1 for 08/2002 to 07/2009.[a]

| | Global mean sea level trend [mm/yr] | Mean sea level trend for latitude $< \|66\|°$ [mm/yr] |
|---|---|---|
| **Greenland** | $0.63 \pm 0.008$ | $0.67 \pm 0.008$ |
| **Antarctica** | $0.26 \pm 0.014$ | $0.27 \pm 0.014$ |
| **Glaciers** | $0.58 \pm 0.027$ | $0.61 \pm 0.027$ |
| **Hydrology** | $-0.20 \pm 0.037$ | $-0.20 \pm 0.037$ |
| **Steric** | $0.35 \pm 0.022$ | $0.37 \pm 0.022$ |
| **GIA** | $-0.16 \pm 0.003$ | $-0.16 \pm 0.003$ |
| **TOTAL (explained)** | $1.45 \pm 0.053$ | $1.56 \pm 0.053$ |
| **TOTAL (Jason-1)** | | $1.94 \pm 0.0046$ |

[a] Please note that the standard deviation of 0.0046 mm/yr for the Jason-1 trend should be interpreted as an instrument-related accuracy propagated to global mean sea level change, which does not account, e.g., for mesoscale current variability and steric sea level change beyond the large-scale pattern we impose in the inversion. In contrast, our inversion misfit of 0.3-0.4 mm/yr suggests that these effects clearly dominate over the instrumental errors in altimetry.

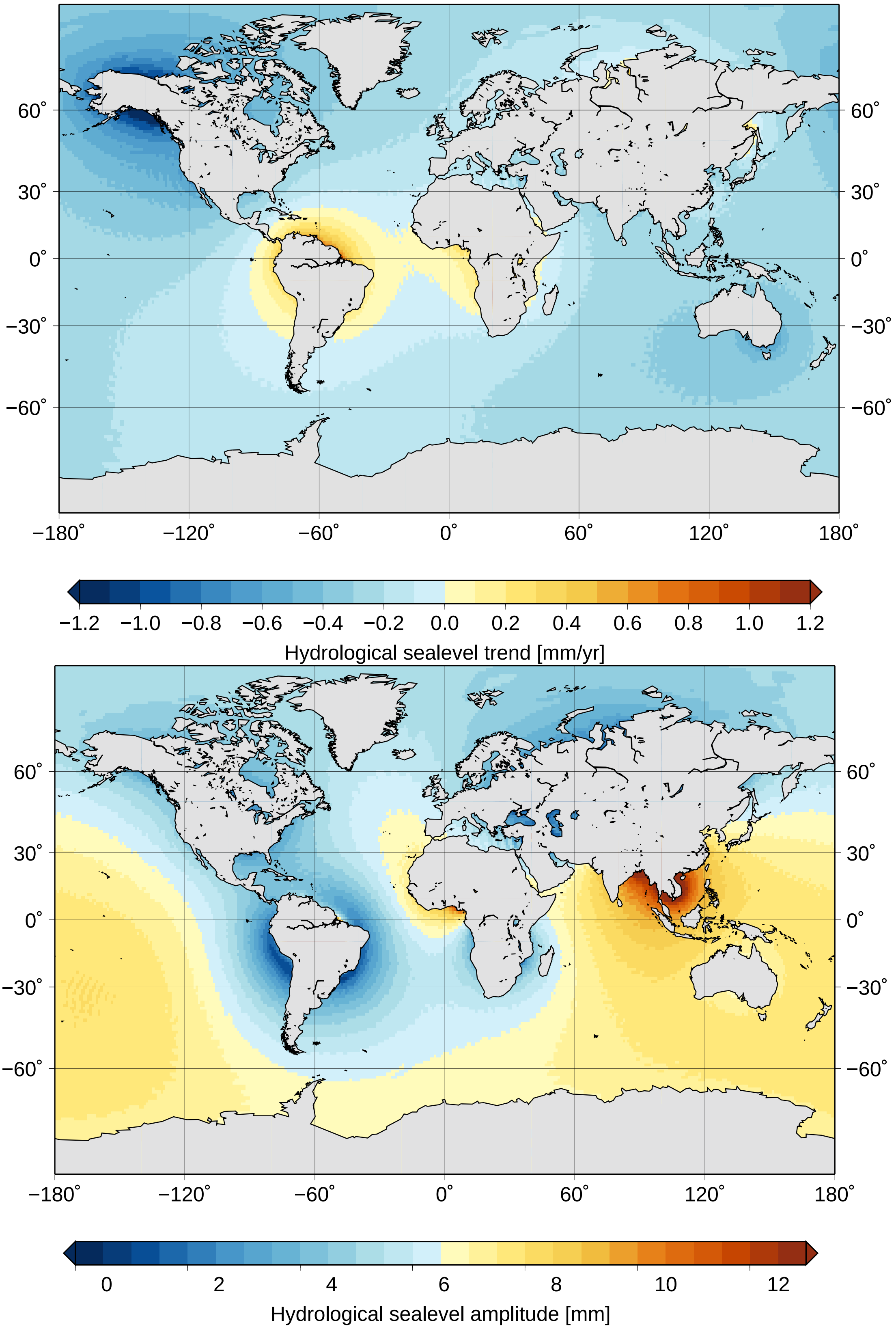


Figure 2: Global sealevel trend and annual amplitude induced by terrestrial hydrological cycle mass changes calculated with a joined inversion of GRACE and Jason-1 data for 08/2002 to 07/2009.

Table 5: Average regional sea level from terrestrial hydrological cycle changes, estimated from GRACE and Jason-1 for 08/2002 to 07/2009.

| | **Sea level trend [mm/yr]** | **Annual amplitude[mm]** |
|---|---|---|
| **Atlantic Ocean** | -0.06 | 5.56 |
| **Pacific Ocean** | -0.25 | 6.94 |
| **Indian Ocean** | -0.23 | 7.55 |